Bureau of Mines Report of Investigations/1987

Acoustic Emission Monitoring of Fracture Development

By Sterling J. Anderson and Peter L. Ruzzi

UNITED STATES DEPARTMENT OF THE INTERIOR

Report of Investigations 9077

Acoustic Emission Monitoring of Fracture Development

By Sterling J. Anderson and Peter L. Ruzzi

UNITED STATES DEPARTMENT OF THE INTERIOR
Donald Paul Hodel, Secretary

BUREAU OF MINES
Robert C. Horton, Director

Library of Congress Cataloging in Publication Data:

Anderson, Sterling J.
Acoustic emission monitoring of fracture development.

(Report of investigations ; 9077)

Bibliography: p. 13-14.

Supt. of Docs. no.: I 28.23: 9077.

1. Rocks--Fracture. 2. Acoustic emission testing. I. Ruzzi, P. L. (Peter L.) II. Title. III. Series: Report of investigations (United States. Bureau of Mines) ; 9077.

TN23.U43 [QE431.6.M4] 622 s [622'.028] 86-607905

CONTENTS

ILLUSTRATIONS

TABLE

UNIT OF MEASURE ABBREVIATIONS USED IN THIS REPORT

dB	decibel	m	meter
ft^3	cubic foot	ms	millisecond
in	inch	µs	microsecond
in^2	square inch	pct	percent
KB	kilobyte	psi	pound (force) per square inch
kHz	kilohertz	s	second
lb	pound	V	volt

ACOUSTIC EMISSION MONITORING OF FRACTURE DEVELOPMENT

By Sterling J. Anderson[1] and Peter L. Ruzzi[2]

ABSTRACT

Through the use of nondestructive testing techniques, the Bureau of Mines is pursuing a goal of improving the efficiency of the rock excavation process. Toward this end, 44 laboratory tests were conducted to identify a practical method of monitoring fracture development in rock, as caused by an excavation tool. An acoustic emission (AE) transducer was used to monitor the test samples as they were loaded. The signal from this instrument was recorded in real time along with the radial and axial loads generated by the fracturing device. Through the review of these signals on a common-time base, it was possible to see the relationship between the developing fracture and the loading conditions.

As a part of the posttesting investigations, samples that were incompletely fractured were sawn and ground to expose the fractures. Visual examination of these samples allowed approximations to be made of the total surface created. Surface area approximations were also made for the completely fractured samples. Quantitative analyses of the AE signals were conducted for comparisons with the calculated surface areas.

[1]Mining engineer.

[2]Mining engineering technician.

Twin Cities Research Center, Bureau of Mines, Minneapolis, MN.

INTRODUCTION

Mining involves a series of independent actions to remove ore from its host rock. One of the actions important to efficient mine productivity is the primary fragmentation process. The Bureau of Mines is conducting basic research directed towards gaining a better understanding of this fragmentation process. In particular, investigations were undertaken to study the relationships between alternative methods of loading rock by excavation tools and the rock's fracture response to loading.

To facilitate these investigations, a nondestructive testing technique called AE monitoring, capable of remotely sensing the phenomena of fracture initiation and propagation, was used. Rock, like many other materials, when stressed, produces an impulse generated by the release of strain energy stored internally within its structure and manifested in the form of elastic waves. These waves travel through the mass, to and then along the surface of the mass. Sensors that respond to these surface waves are the heart of the AE monitoring technique. Differing sensing techniques have been used, including optical- and capacitance-style transducers (1).[3] Piezoelectric-style transducers are the most commonly used and have the greatest sensitivity with the ability to detect displacements as small as 10^{-12} m (2). Sources of AE include dislocation movements, phase transformations, friction mechanisms, and fracture formation and extension. Of these, friction mechanisms and fracture formation are of greatest significance. Fracture initiation occurs at points within a mass where local stresses exceed a critical level. The resulting fracture formation creates new surfaces, and a burst of strain energy is released that is partly transformed into AE. AE attributed to friction mechanisms occurs within the fracture by the sudden relative movement of its adjacent surfaces (3). Another friction mechanism that can result in AE activity is tool-rock interaction.

Traditionally, AE monitoring techniques have been used to monitor microseismic activity in the fields of ground control and tectonics (4-7). More recently, AE equipment has been developed that can monitor the failure of materials on a much smaller scale (2). Researchers have been employing this technique to study the failure mechanisms of rock by examining the AE signal's characteristics (8-9), to identify mechanical properties by examining the rate of AE (10), and in general to evaluate the usefulness of the AE signals generated in these studies. Controversy remains over the interpretation of AE signals (11); however, there exists a consensus in agreement among these authors (1-11), and the authors of this report, that AE monitoring is an excellent technique for remotely sensing the failure of rock.

In this laboratory investigation, an assumption was made that a relationship should exist between the AE activity generated during fracturing and the amount of fracture surface area created. Based on this assumption, experiments were conducted in an attempt to provide a method for remotely characterizing the extent of fracturing caused by an excavation tool. To achieve this goal, rock samples were fractured while being monitored by a single AE transducer. The extent of fracturing was varied from sample to sample, and in many trials, fractures were purposely arrested within the sample. In the trials where arrested fractures were produced, the samples were sawn and ground so that visual examinations of the fractures could be made. From visual examinations of all the samples, fracture surface areas were calculated. Correlations were then made between the calculated fracture surface areas and the summations of the corresponding AE signal event counts and event amplitudes. As a complimentary goal, the AE signal was

[3]Underlined numbers in parentheses refer to items in the list of references preceding the appendix.

also studied in its real-time context to establish its usefulness in delineating the loading conditions under which fracture initiation and propagation occurs.

APPARATUS AND MATERIALS

Sample loading was accomplished with an in-hole fracture device (fig. 1). This laboratory device was designed in-house (12), and its design is based upon a primary excavation tool developed by the Institute CERAC in Switzerland (13). The in-hole fracture device operates from within a previously drilled hole and is hydraulically powered. The device is made up of a special hydraulic cylinder containing two pistons, each capable of independent movement, and components that load the rock from within a predrilled hole. From their rest positions, (fig. 2), the two pistons travel toward each other within the cylinder. The wedge component is attached to the forward piston, which draws it into the cylinder body. This action causes the leaves of the feather components to deflect radially outward, come into contact with the hole wall, and anchor the device within the rock mass under a radial load, much like a mechanical rock bolt. The thrust-rod component is attached to the second piston and is advanced by its action, causing the rod to contact the hole bottom and develop a load. This axial load produces tensile stress in the rock sample, causing the rock surrounding the device to be torn free from the mass as it moves outward with the device (fig. 3). If done carefully, slow fracture growth and arrested fractures can be generated.

By means of a load cell, a calibration, with an error of ±1 pct, was made of the pressure-load relationships for each of the two functions the device performs. As expected, linear relationships were developed by these trials with system losses due to hydraulic fluid flow and mechanical friction amounting to about 70 psi in both cases.

The pressure-load relationships developed were

$$R = 9.76\ P_1 - 681$$

and

$$A = 3.42\ P_2 - 248,$$

where R = radial load, lb,

A = axial load, lb,

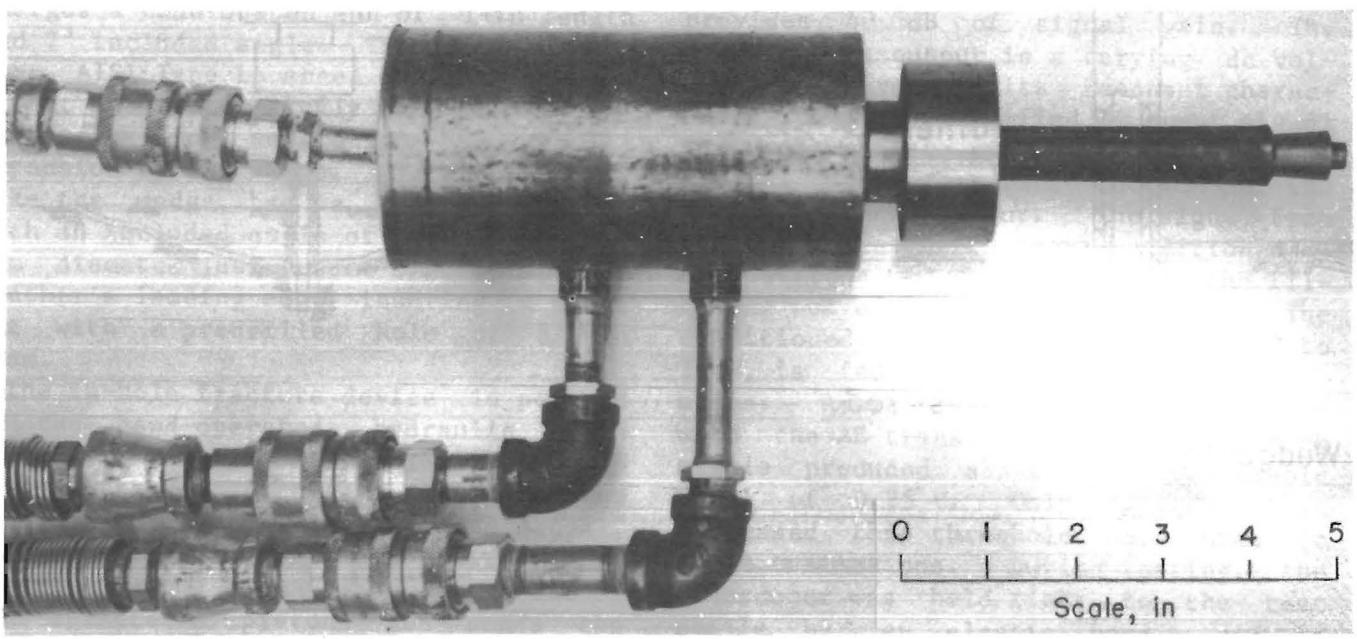

FIGURE 1.—In-hole fracture device.

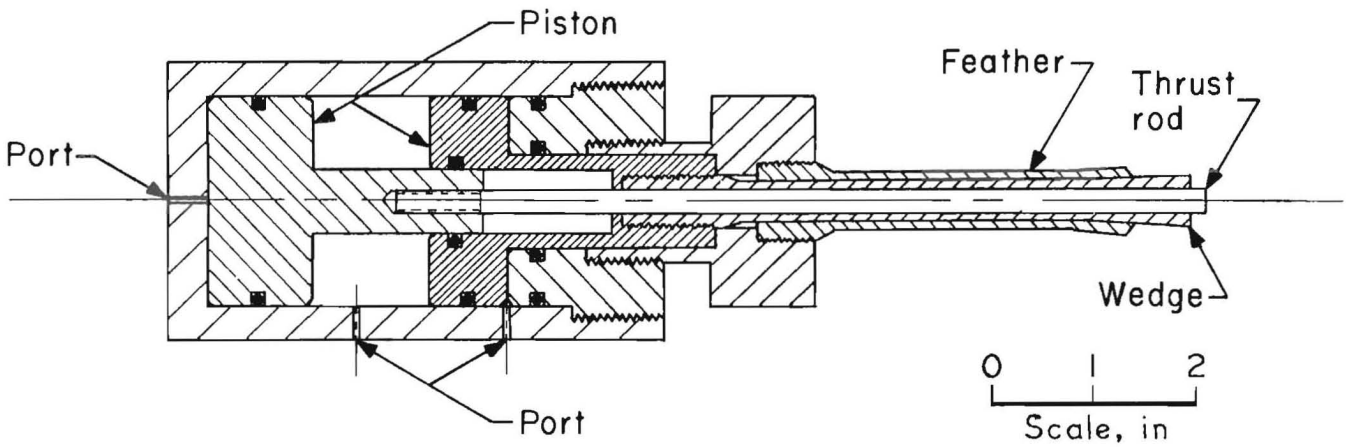

FIGURE 2.—Fracture device detail.

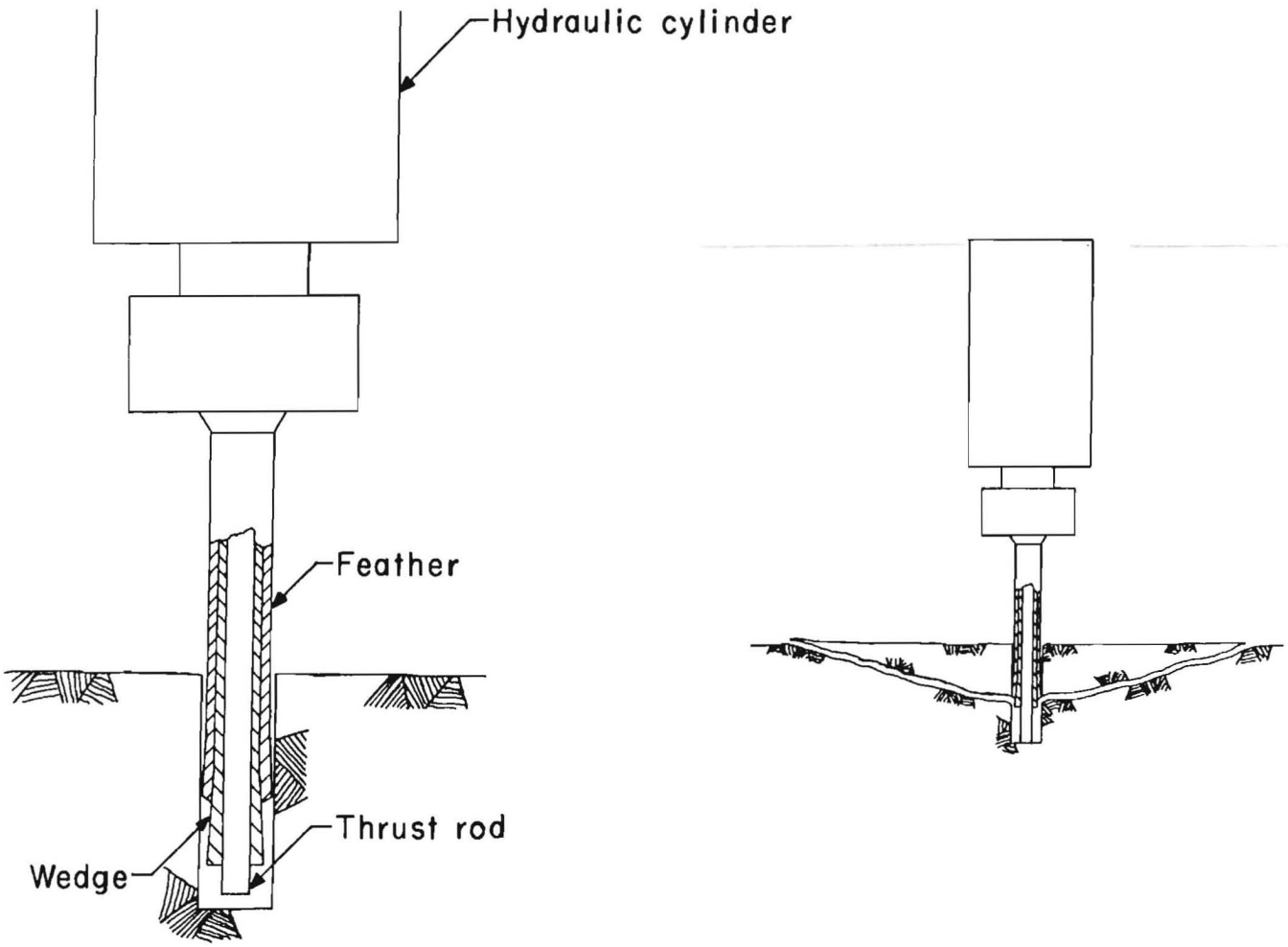

FIGURE 3.—Fracture device action.

P_1 = pressure driving piston to where wedge is attached, psi,

and P_2 = pressure driving piston to where thrust is attached, psi.

The axial load is simply a function of the effective area of the piston. The radial load is much greater and is a function of not only the effective area of the piston driving the wedge, but also of the wedge angle and the efficiency with which the wedge and feather translate this action into the radial load. The feather, wedge, and thrust rod components of the in-hole fracture device are the load-transmitting members, and their design is critical for the effective operation of the device.

Tool steels that were heat treated for increased hardness and strength were used for these three concentric components. The centrally located thrust rod, made from AISI Type 02 steel and hardened to 56 Rc, has a 5/16-in diam, a 7/16-in stroke, and works under loads up to 6,500 lb. The wedge, made from AISI Type 02 steel and hardened to 56 Rc, has a 11/16-in stroke and works under loads up to 5,000 lb. This component is positioned with sliding clearances between the feather and thrust rod, and it resembles a thick-walled tube from which emerges a cone-shaped end of 1-in length and 7° included angle. The feather, made from AISI Type L6 steel and hardened to 50 Rc, is split axially into four equal components for separation and radial expansion by the wedge. This component, like the wedge, has a cone-shaped end, with an included angle of 3° and a maximum diameter just under 5/8 in at the feather's leading edge, insuring a close fit with a predrilled hole of 5/8-in diam.

The in-hole fracture device is powered by two hand-operated hydraulic pumps (fig. 4). One is a single-speed pump with a manual load-release valve, and the other is a two-speed pump with a manual, three-position, four-way, directional control valve. Each pump actuates one of the splitter's pistons and sends the return fluid to the pump equipped with

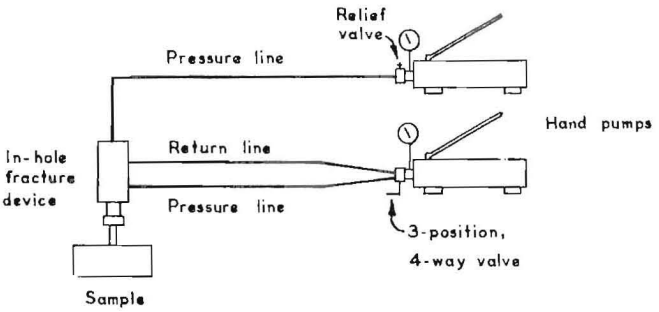

FIGURE 4.—Hydraulic circuit.

the four-way valve. Repositioning of the four-way valve and release of the relief valve allows the two-speed pump to return the pistons to their rest positions. The pumps offer excellent control over the fluid pressures supplied to the cylinders; they allow for slow pressurization and holding of the pressure without attendance. For more information regarding this device and its use, see reference 12.

Pressures relating to the radial and axial loads were monitored by gauges and pressure transducers mounted in the supply lines. Signals from these transducers were fed into a digital oscilloscope where they were recorded as a function of time.

The piezoelectric AE transducer used in these tests has a resonant frequency of 60 kHz and an integral preamplifier that provides 40 dB of signal gain. The transducer's output is a varying dc voltage that envelopes its resonant characteristic. The amplified AE event signal features a fast rise time and an exponential decay that is a function of the ringdown of the sensor. The signal from the transducer is further conditioned by an additional 60 dB of gain and the filtering out of its negative portion. The conditioned signal, with a range of 0 to 15 V, is fed into the digital oscilloscope. Ambient AE signal readings taken with the AE transducer held to the rock sample produced a baseline threshold level of 0.25 V. Only AE events that surpassed this threshold were used in these evaluations. During testing, the transducer was held tight to the test sample by an elastic band, and no couplant was used.

Each of the transducers, AE and pressure, sent their signals to the digital oscilloscope via coaxial cable where the signals were captured in real time and postdata acquisition processing took place (fig. 5). The digital oscilloscope is a four channel unit with 12-bit resolution and 32 KB of memory per channel. In producing a single data point, the unit takes an average of the analog input signal over the sampling interval. The minimum sampling interval available is 10 μs; however, a sampling interval of 20 ms was used in these tests. This sampling interval was used to allow the oscilliscope to capture the test data in full. This sampling technique, however, did preclude full AE event characterization, making it possible to identify the event only by its real-time occurence and amplitude. The digital oscilloscope is capable of triggering its data acquistion by a change in voltage in any one of the four channels. The unit also features a disk drive for data storage and retrieval, an X-Y plotter, and postdata acquisition processing capabilities.

Testing was conducted in blocks of Salem limestone. This rock has a bioclastic texture and is made up of shells of gastropods, crinoid stems, and caliches that are cemented together by crystalline calcite. The proportions of these phases are approximately 69 pct fossiliferous calcite to 31 pct calcite cement (14). See table 1 for a partial listing of Salem limestones physical properties.

For the tests, each of the Salem limestone samples was similarly prepared. Large blocks were first cut into 8- by 8- by 4-in sample size, then predrilled with

TABLE 1. - Physical properties of Salem limestone (Indiana limestone, Bedford, IN)

Strength, psi:	
Compressive	9,991
Tensile	502
Shore hardness scleroscope units	32
Apparent density, slugs/ft^3	4.635
Modulus, 10^6 psi:	
Static Young's	4.4
Dynamic Young's	4.65
Shear	2.32
Poisson's ratio	0.33

NOTE.--Source: reference 15.

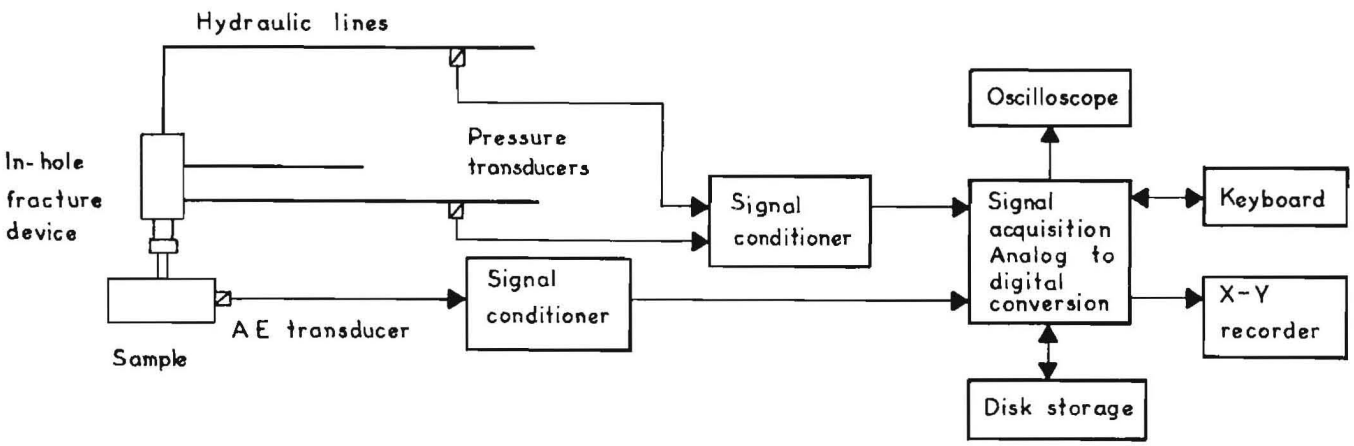

FIGURE 5.—Instrumentation.

a 5/8-in-diam bit to a depth of 1-1/2 in to receive the in-hole fracture device. These holes were centered on an 8- by 8-in face of the sample, and because of the required overdrilling, provided for a fracture initiation zone at a depth of 3/4 in from the block's surface. These holes had an orientation parallel with the bedding (fig. 6) so that the generated fractures ran across the bedding. This orientation was selected because earlier work with the device showed that the fractures may run preferentially down the bedding planes if the device or hole orientation is perpendicular to them.

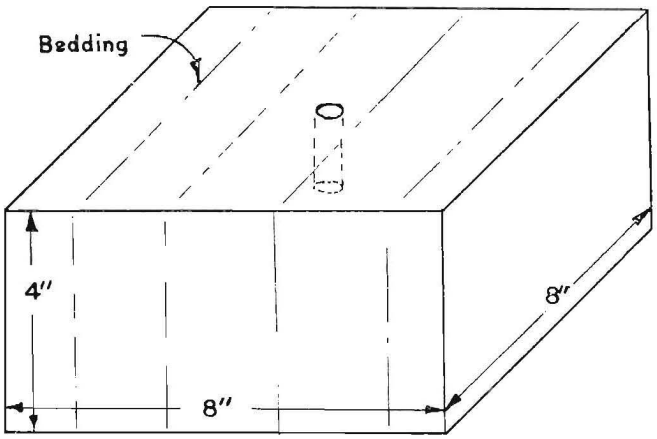

FIGURE 6.—Test sample.

PROCEDURES

Test preparations were initiated by placing a sample on the test bed. In order to isolate the sample from extraneous vibrations, the test bed consisted of a 24- by 19- by 31-in block of limestone that was supported over a standard wood framework floor resting on a concrete slab. The sample was further isolated from the block by a 1-in-thick felt pad. With the sample in place on the bed, the AE transducer was positioned and the in-hole fracture device was set in place. To minimize movement by the in-hole device, it was mounted in a supporting stand (fig. 7). When all equipment was in place, a check was made of the digital oscilloscope settings, and the oscilloscope was set to trigger and capture data based on the rise in radial load. The hand pumps were then operated supplying the radial and axial loads, and the fracture event was monitored. During testing, loads were applied at similar rates until AE signal levels were indicative of fracture development. At that point, the loading was slowed to facilitate slow fracture growth and/or arrested fractures. Arrested fractures were produced in these tests to provide a variety of fracture surface areas with which to correlate the AE activity. Typically, the tests were conducted in under 60 s. At test conclusion, the three channels of data corresponding to the signals from the AE activity and two pressure signals were stored on a floppy disk and plotted together by the X-Y plotter.

For those tests where the fractures had been arrested within the sample, the blocks were sawn into quarters, and the eight newly created surfaces were ground (fig. 8) for viewing. The new surfaces were examined under a stereo microscope (X 70) for the extent of primary fracture development and for damage in the anchoring zone. From these observations, estimates were made of the surface area developed by the primary fracture.

The following method was used to estimate the surface area of the fracture: The extent of fracturing was measured from the upper surface of the quartered blocks (t) and from the edge of the drill hole at the fracture initiation point to the crack tip (d) (fig. 9) for all eight of the newly created faces of the original samples. Assuming that the fracture length was the same for the matching faces, the longest measurement of the pair was used for the fracture length

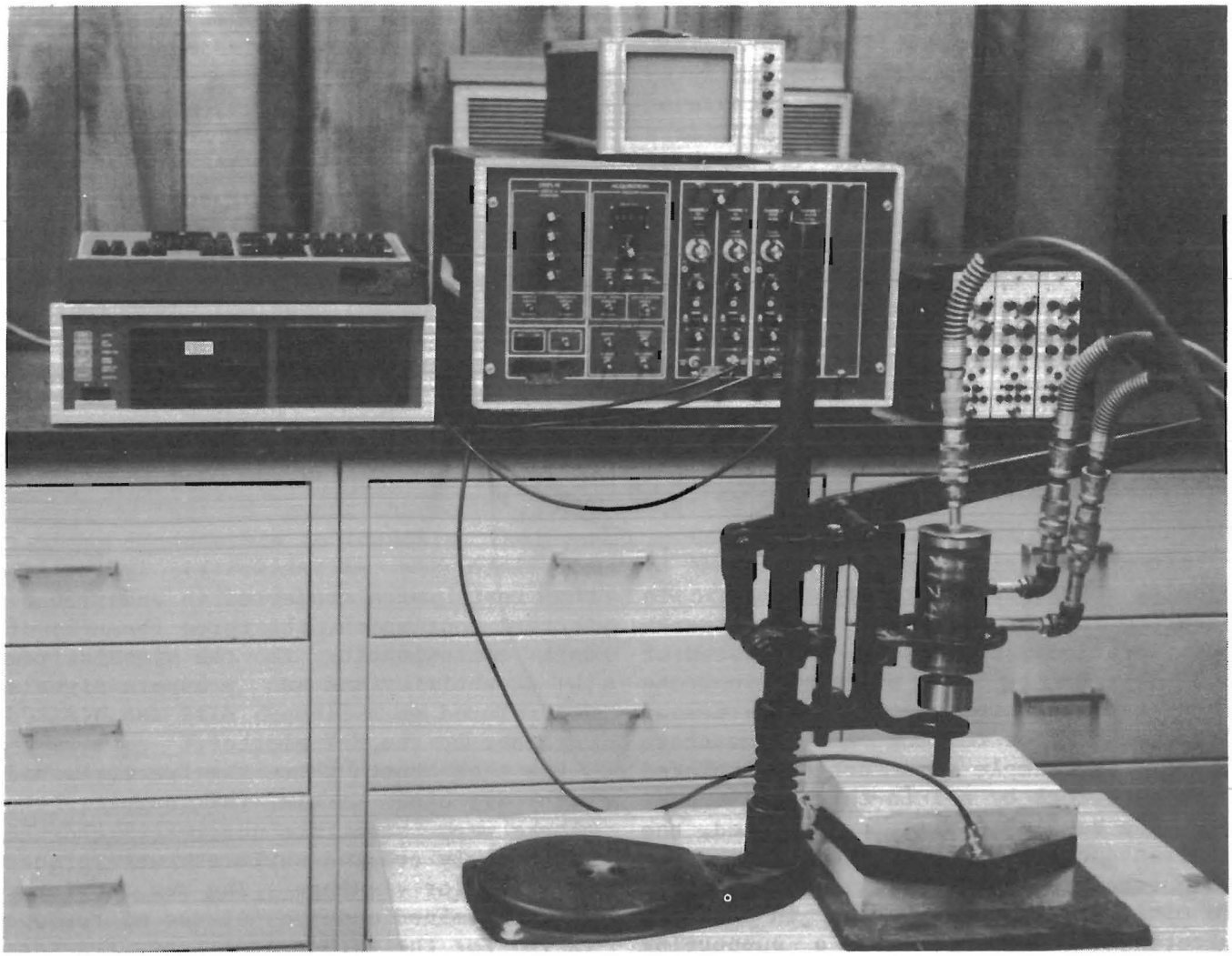

FIGURE 7.—Laboratory facility.

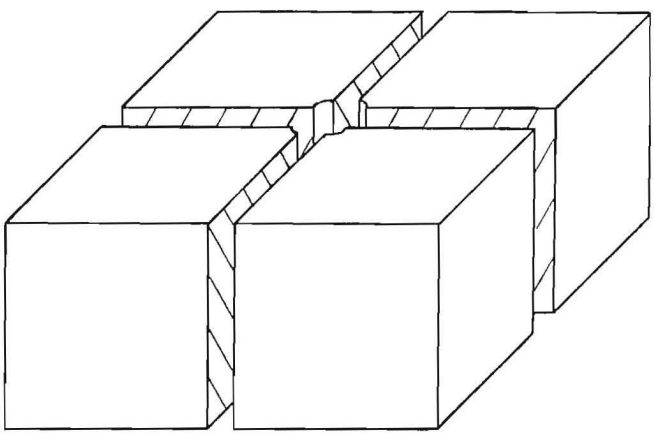

FIGURE 8.—Posttesting sample preparation, the shaded surfaces are those prepared for viewing.

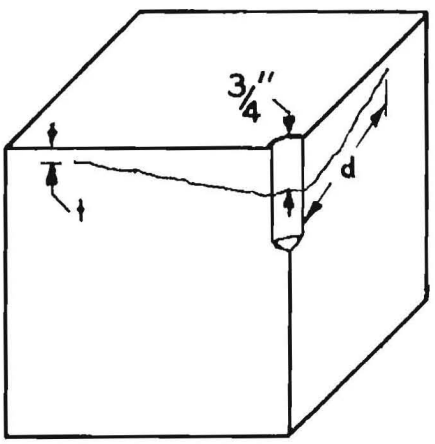

FIGURE 9.—Surface area of fracture construction detail.

in that direction. The four orthogonal measurements were then averaged to establish an average fracture length for the block. At this point, the fracture was assumed to have a conical profile starting at the edge of the drill hole, at a 3/4-in depth from the surface of the block, and ending at the crack tip, with a linear distance equal to the block's average. This linear approximation was then used in the following surface-area-by-revolution formula to calculate an approximation for the fracture surface area.

$$\text{Area} = 2\pi\ (1+a^2)^{1/2} \left(\frac{a}{2}n^2 + bn\right),$$

where $a = \frac{(d^2-n)^{1/2}}{n}$,

b = drill-hole radius, 5/16 in,

n = 3/4 - t, in,

d = linear approximation for the crack length, in,

and t = depth of the crack tip measured from the surface, in.

In the tests where the fractures extended to the surface, freeing a part of the mass, a slightly different method was used to estimate the surface area. The distance that the fracture surfaced from the edge of the drill hole was measured in the same four orthogonal directions used in the cases where the blocks were first quartered (fig. 10). These measurements were then averaged to establish a block average. The fracture was assumed to have the same conical profile described earlier, and the same formula was used to calculate an approximation for the fracture surface area. The difference lies in the definitions of the variables. Restating the formula:

$$\text{Area} = 2\pi\ (1+a^2)^{1/2}\left(\frac{a}{2}n^2 + bn\right),$$

where $a = \frac{c}{n}$,

b = the drill hole radius, 5/16 in,

n = the distance from the surface to the fracture initiation point, assumed to be 3/4 in,

and c = the average distance from the edge of the drill hole to the surfacing of the fracture, in.

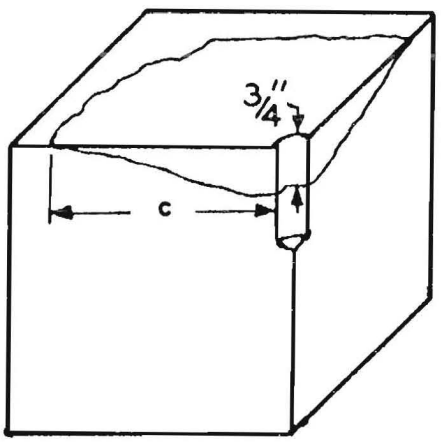

FIGURE 10.—Surface area of fracture construction detail for completely fractured sample.

DISCUSSION OF RESULTS

One of the objectives of this work was to provide a method of demonstrating the correspondence between the loading and the initiation and propagation of fractures. Towards this end, the AE monitoring worked extremely well, providing the capability to determine when failure was taking place. In posttesting review of the AE and loading history on a common-time base, it was possible to accurately describe the loading levels at discrete failure events.

Figure 11 displays the AE signal relationship for a typical load from test 11. Region A of this figure displays the application of the radial load and the corresponding AE activity. In four separate trials, the extent of damage, or fracture development due to the radial load alone, was investigated. Within these tests, typical radial loads were applied. As with the test samples containing arrested fractures, these test blocks were quartered and inspected under a microscope for the extent of damage. In all four trials, a damaged zone containing both crushed material and fractures was formed at the feather-limestone interface that extended for a radius of approximately 3/16 in from the line of contact. The fractures contained in this zone were roughly parallel to the compressive anchoring load, and it appeared that under additional loading, these fractures coalesced to form the primary fracture. Indeed, primary fractures parallel to the compressive load can be run under this load alone, even though this loading was intended only to provide sufficient grip for the mass to be fractured by the axial

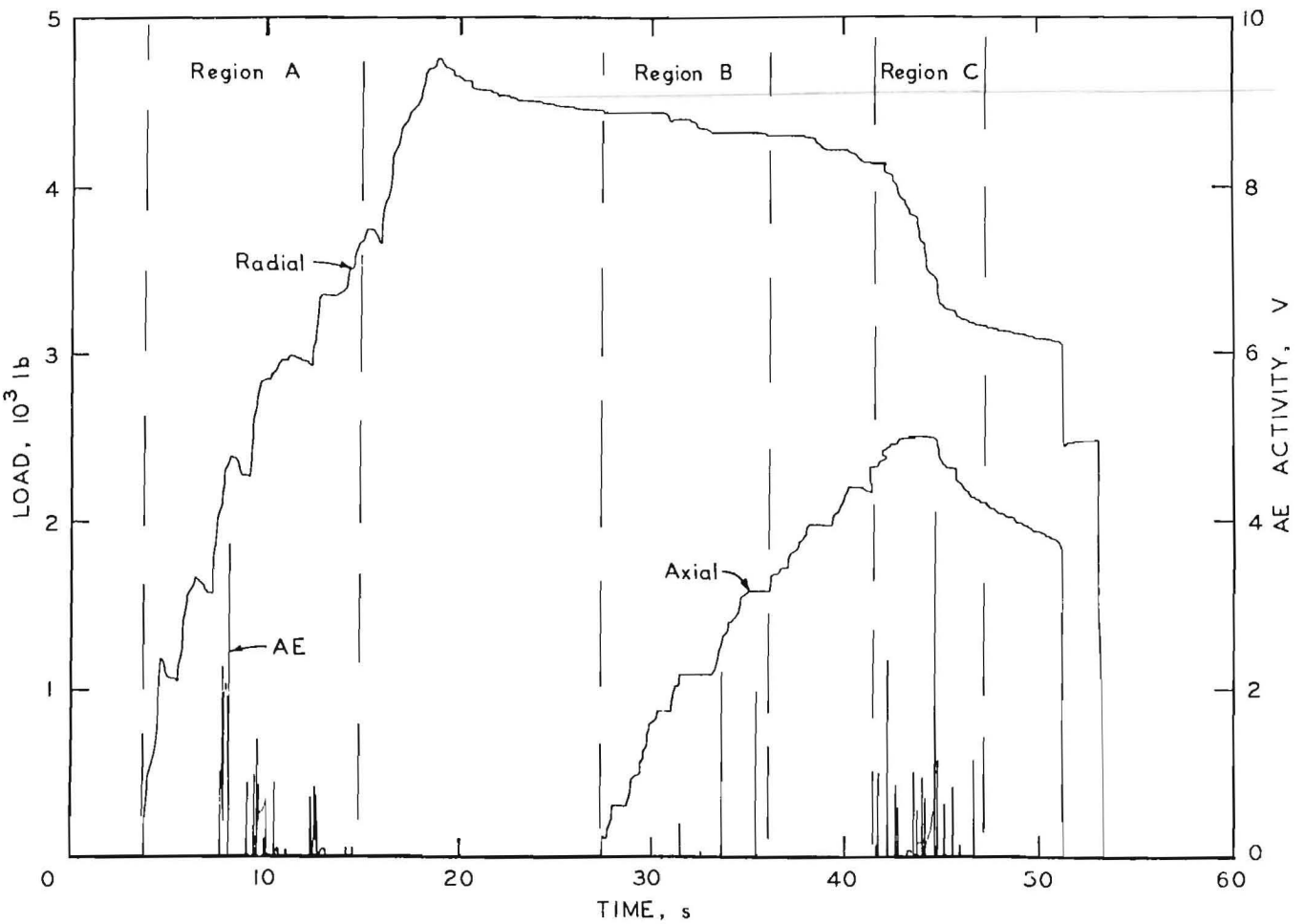

FIGURE 11.—Typical time-base fracture history.

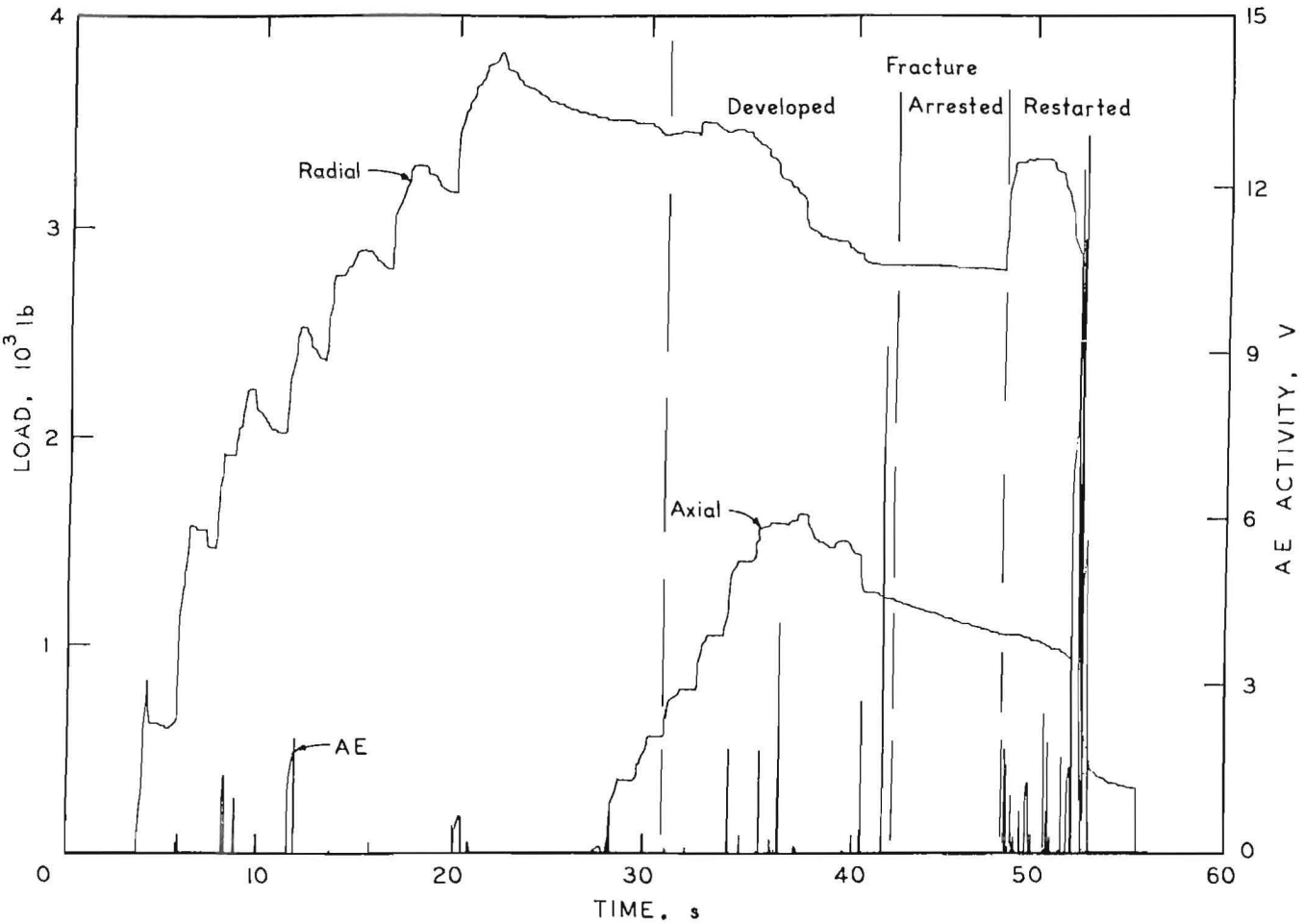

FIGURE 12.—Load-AE signal relationships.

load. See the tests with the zero axial load in the appendix table for examples of these trials. The AE activity associated with region A is, therefore, attributable to a combination of sources, including friction caused by tool-rock interaction that caused by-grain movement during crushing, and fracture formation and extension.

Region B in the figure depicts the reaction of the sample to the application of the axial load. Because the thrust-rod component is loading against the bottom of the hole, AE activity is sometimes present in response to the compressive loading at this interface and to relative movement at the feather-rock interface. Region C in the figure shows the development of the primary fracture. Note the relationship between the loads and the restarting of arrested fractures; figure 12, "test 26" shows that with an increase in radial load, the arrested fracture is restarted under loading conditions that are less than those previously required to start the fracture. This phenomena is a function of the distance the fracture front has proceeded from the point of application of the load and the resistance to fracturing in the immediate vicinity of the fracture front. The loading system used in the tests stores energy that is primarily released through failure of the sample. The figure shows the relationship between the falling loads and the discrete AE events, and thereby, the load and fracture propagation relationship. Arrestment of the fracture is indicated by the periods in the AE signal containing no activity.

Another objective of this work was to provide a remote method of characterizing the fracture development in real-time, with the hypothesis being that a

relationship should exist between the number of AE events and the amount of surface area created. Within the various tests, the radiating fracture front was arrested at different stages of its development, as indicated by the fracture surface areas given in table A-1. The number of event counts related to the total number of threshold crossings by the AE activity were summed and compared to the fracture surface area created in each test. In a comparison of the total number of counts, or the sum of counts over the entire test, with the fracture surface area, no correlation was found. In an additional comparison, the counts relating to the AE activity over region C of the loading history were summed and compared to the fracture surface area created in each test where axial loads were applied (fig. 13 top). In this comparison of region C activity to the surface area, some of the AE signal variation attributable to mechanisms such as crushing and tool-rock interactions can be bypassed. The figure shows a trend in the data that suggests a correlation. Using linear-regression techniques, the relationship between the surface area and the event counts over region C of the loading history were evaluated. The following relationship was derived:

$$AEC = 3.45\ SA + 77.07$$

(with $r^2 = 0.26$; see below),

where SA = calculated surface area, in,

r^2 = coefficient of determination,

and AEC = event counts relating to the AE activity over region C of the loading history.

In this relationship, r^2 is the proportionate reduction of total variation associated with the use of the independent variable. Thus, the larger the coefficient, the greater the total variation reduced by introducing the independent variable.

In search of a better correlation, event energy based on the square of the event amplitude was summed and compared to the fracture surface area. The correlations produced were only slightly better than the event count sum comparisons. A better correlation was produced when event amplitudes multiplied by the sampling interval were summed and compared to the calculated fracture surface area (fig. 13, bottom). As with the comparsion using the event count sum, no correlation was found when the comparison was made over the entire test. However, when the comparison was made with the region C AE activity, the following relationship was derived:

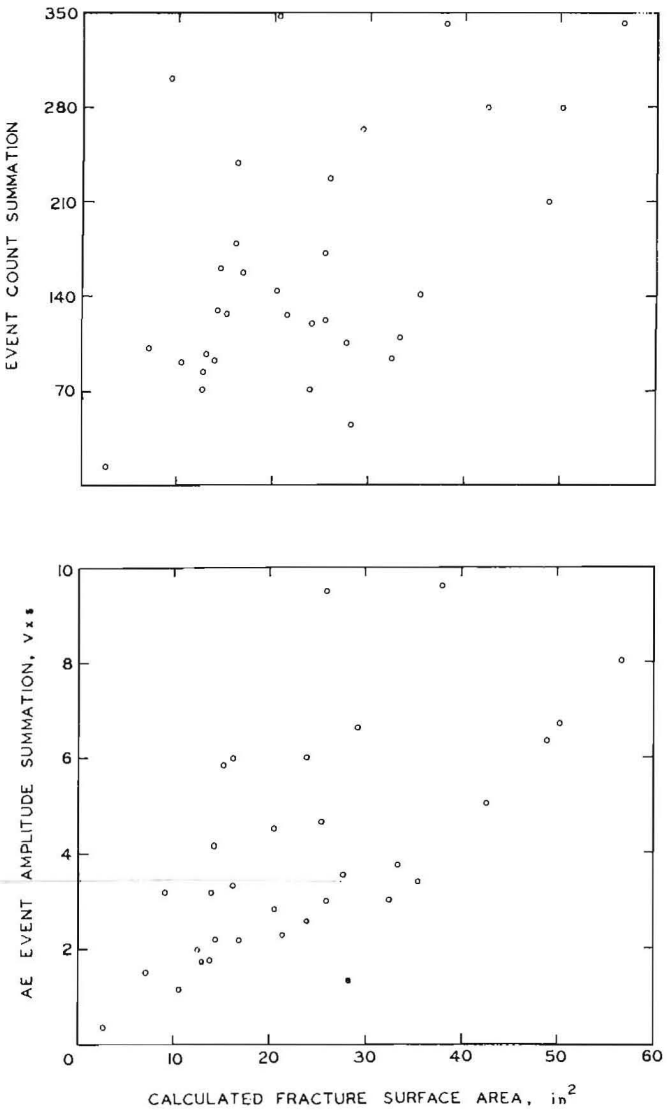

FIGURE 13.—Surface area versus event count sum for region C (as shown in figure 11) AE activity (top) and surface area versus event amplitude summation for AE activity in same region (bottom).

$$SAEA = 0.12SA + 1.23, \quad r^2 = 0.40,$$

where SAEA = sum of the AE event amplitudes times the sampling-interval of 20 ms over region C of the loading history.

Thereby, the creation of fracture surface was found to explain 40 pct of the variation in the summation of the event amplitudes. In a null-hypothesis test after Chatterjee (16), this relationship was found to have significance with 99 pct confidence. The appendix table gives the data for these comparisons.

SUMMARY AND CONCLUSIONS

With the single-transducer AE monitoring system used in these tests, a relationship between the AE signal and the extent of fracturing could not be developed at this time. Better correlation was expected, and procedures and materials were reexamined to help clarify the perceived problem. An obvious proposal is that the inhomogeneity of Salem limestone contributed to the problem. The size and type of fossil forms that make up the mass and the number of voids present can change greatly from one area to another within a sample. Another consideration is the degree of coupling. Coupling was achieved through the use of an elastic strap holding the AE transducer securely to a side face of the block. However, because no couplant was used to enhance the transmittal of the elastic wave to the transducer, and because the degree of coupling was not checked before each test, the assumption that the degree of coupling was constant for each individual test may not be valid. In ongoing work, these problems will be addressed through the use of rock samples that are more homogeneous and isotropic and through the development of a method of calibrating the degree of coupling. A final consideration is the system's inability to distinguish between actual fracture events and AE events attributable to tool-rock interactions. Future studies will use AE source location techniques employing multiple transducers to locate the sources of AE events (17). This technique should provide the means by which actual fracture events can be distinguished from tool-rock interaction noise.

However, this work has confirmed the acute sensitivity of AE transducers to the failure of material. This monitoring technique is very successful because of the excellent feedback the AE transducer provides on the rock response to loading. Through the use of these instruments and real-time monitors, load and fracture development relationships can be accurately described.

REFERENCES

1. Scruby, C. B. Acoustic Emission Measurements Using Point-Contact Transducers. J. Acoust. Emiss., v. 4, No. 1, 1985, pp. 9-18.

2. Scala, C. M. Acoustic Emission Sensors. J. Acoust. Emiss., v. 2, No. 4, 1983, pp. 275-279.

3. Bruel and Kjaer Instruments, Inc. (Cleveland, OH). Technical Review, Acoustic Emission. No. 2, 1979, 40 pp.

4. Hardy, R. H. Jr., F. W. Leighton (ed.). Proceedings of the First Conference on Acoustic Emission/Microseismic Activity in Geologic Structures and Materials (PA St. Univ., Univ. Park, PA, June 9-11, 1975). Trans. Tech. Publ., 1977, 491 pp.

5. Hardy, R. H. Jr., F. W. Leighton (ed.). Proceedings of the Second Conference on Acoustic Emission/Microseismic Activity in Geologic Structure and Materials (PA St. Univ., Univ. Park, PA, Nov. 13-15, 1978). Trans. Tech. Publ., 1980, 490 pp.

6. _____. Proceedings of the Third Conference on Acoustic Emission/Microseismic Activity in Geologic Structures and Materials (PA St. Univ., Univ. Park, PA, Oct. 5-7, 1981). Trans. Tech. Publ., 1984, 805 pp.

7. Drnevich, G. (ed.). Acoustic Emissions. ASTM Spec. Tech. Publ. 750, 1981, pp. 4-94.

8. Fonseka, G., G. Murrell, and P. Barnes. Scanning Electron Microscope and Acoustic Emission Studies of Crack Development in Rocks. Int. J. Rock Mech. Min. Sci., v. 22, No. 5, 1985, pp. 273-289.

9. Ohnaka, M. Acoustic Emission During Creep of Brittle Rock. Int. J. Rock Mech. Min. Sci., v. 20, No. 3, 1983, pp. 121-134.

10. Gowd, T. N. Factors Affecting the Acoustic Emission Response of Triaxially Compressed Rock. Int. J. Rock Mech. Min. Sci., v. 17, No. 4, 1980, pp. 219-223.

11. Niwa, Y., S. Kobayashi, and M. Ohtsu. Source Mechanisms and Wave Motions of Acoustic Emission in Rock-Like Materials. Paper in Acoustic Emission/ Microseismic Activity in Geologic Structures and Materials, ed. by R. H. Hardy, Jr., and F. W. Leighton (Proc. Third Conf. PA St. Univ., Univ. Park, PA, Oct. 5-7, 1981). Trans. Tech. Publ., 1984, pp. 101-115.

12. Anderson, S. J., D. E. Swanson. Laboratory Testing of a Redial-Axial Loading Splitting Tool. BuMines RI 8722, 1982, 26 pp.

13. Cooper, G. A. Method and Apparatus for Breaking Hard Compact Material Such as Rock. U.S. Pat. 4,099,784, July 11, 1978.

14. Krech, W. W., F. A. Henderson, K. E. Hjelmstad. A Standard Rock Suite for Rapid Excavation Research. BuMines RI 7865, 1974, 29 pp.

15. Morrell, R. J., W. E. Bruce, and D. A. Larson. Tunnell Boring Technology. BuMines RI 7410, 1970, 32 pp.

16. Chatterjee, S., and B. Price. Regression Analysis By Example. Wiley, 1977, 228 pp.

17. Dowding, C. H., L. Samama, and S. P. Shah. Location of Acoustic Emissions During Fracture of Slightly Anisotropic Granite. Paper in 26th U.S. Symp. Rock Mech., ed. by E. Ashworth (Proc. Conf. SD School Mines and Tech., Rapid City, SD, June 26-28, 1985), and A. A. Balkemer, 1985, pp. 731-738.

APPENDIX.--TEST DATA

Test	Maximum load, lb		Surface area, in^2	Event count sum		Event amplitude sum,[3]	
	Radial	Axial		Total AE	Area c, AE activity	Total AE	Area c, AE activity
1	3,812	1,803	23.90	168	70	3.99	2.57
2	4,207	1,681	35.37	310	140	6.17	3.49
3	3,092	913	25.84	550	226	14.54	9.48
4	4,303	0	18.31	459	(1)	4.71	(1)
5	2,940	0	.31	481	(1)	14.57	(1)
6	3,955	2,718	29.27	521	264	8.71	6.59
7	5,137	2,016	48.99	309	210	7.20	6.34
8	5,084	2,275	50.11	373	278	8.59	6.84
9	4,379	2,454	28.15	74	44	1.52	1.30
10	4,641	1,858	32.32	122	94	3.36	3.06
11	4,012	2,504	16.90	413	155	5.44	2.19
12	3,726	1,873	14.17	189	129	4.54	4.17
13	3,807	1,776	21.52	363	126	4.36	2.27
14	4,436	1,687	56.66	482	344	9.47	8.01
15	5,961	584	15.15	344	128	8.25	5.82
16	4,655	0	8.32	186	(1)	5.16	(1)
17	5,137	0	31.14	253	(1)	4.47	(1)
18	4,446	1,133	33.37	132	108	3.98	3.74
19	4,927	2,130	13.98	119	91	3.59	3.17
20	5,480	0	26.11	154	(1)	4.06	(1)
21	5,218	2,003	12.97	152	96	2.20	1.69
22	4,836	2,227	16.17	230	178	6.38	5.94
23	5,008	2,078	12.59	106	71	2.17	1.94
24	4,117	0	2.07	132	(1)	1.30	(1)
25	4,164	2,380	25.32	273	171	6.05	4.61
26	3,087	1,576	20.47	677	348	9.81	4.52
27	2,439	0	.06	452	(1)	12.62	(1)
28	2,935	1,682	20.47	320	145	5.55	2.80
29	3,750	1,504	27.74	336	106	5.49	3.51
30	3,240	1,946	24.02	462	120	9.95	5.90
31	6,500	1,235	6.99	235	103	2.86	1.50
32	3,616	1,576	10.45	197	90	2.01	1.13
33	4,217	983	14.58	275	159	3.38	2.19
34	5,241	1,292	37.91	466	341	10.51	9.55
35	3,492	1,876	42.41	279	249	5.28	5.07
36	3,578	1,510	25.58	199	122	3.59	2.96
37	3,979	1,978	13.60	135	84	2.37	1.74
38	4,117	1,532	2.58	44	14	.62	.36
39	5,980	1,719	16.21	396	238	5.21	3.30
40	2,887	1,395	9.09	523	299	9.59	3.19
41	3,211	0	(2)	318	(1)	7.96	(1)
42	4,846	0	(2)	191	(1)	2.27	(1)
43	3,807	0	(2)	60	(1)	.44	(1)
44	3,778	0	(2)	159	(1)	.22	(1)

[1]No axial load for these tests.
[2]Primary fracture not developed.
[3]Voltage times time (in seconds).

INT.-BU.OF MINES,PGH.,PA. 28442

U.S. GOVERNMENT PRINTING OFFICE. 1987 605 017 60023